Large swings in the forward-backward super-radiant emission direction from a nearly inverted ensemble of a three-level cascade system

Jamal T. Manassah*

Department of Electrical Engineering, City College of New York, New York, New York 10031, USA

(Received 27 July 2015; revised manuscript received 2 November 2015; published 16 February 2016)

I show unambiguously that, in a slab geometry, the direction of emission of the super-radiant pulse from the lower two levels' transition in an ensemble of a three-level cascade homogeneously broadened atomic system, which was initially prepared in a nearly fully inverted coherent state, exhibits high sensitivity to the value of the initial atomic population for the case that the slab thickness is equal to $n\lambda_0/2$ (n is an integer and λ_0 is the wavelength of the atomic transition). Specifically, I compute, in this regime, the swings in the ratio of the forward over backward fluxes for both transitions as a function of the initial population of the highest energy level.

DOI: 10.1103/PhysRevA.93.023820

I. INTRODUCTION

The proof of the existence of an anomalous forward-backward asymmetry in the solutions of the super-radiant problem [1] from an ensemble of identical homogeneously broadened two-level atoms arranged in a slab geometry has posed for the longest time a numerical computational challenge and a physical puzzle to its origins. Recently, using the expansion of the complete set of the Maxwell-Bloch (MB) system of equations, in the basis formed by the eigenfunctions of the one-dimensional (1D) Liénard-Wiechert kernel [2,3], I obtained stable numerical solutions [4] to this problem in the targeted regime of the initial population of the excited state. I showed that the large swings in the forward-backward super-radiant emission direction occur in a narrow strip of the values of the slab thickness, namely when equal to $n\lambda_0/2$ (n is an integer >2 and λ_0 is the wavelength of the atomic transition). The two-level model solved included the atom's interaction with all modes of the electromagnetic field (i.e., no single mode assumption for the field is made) and makes no rotating wave approximation (RWA) or slowly varying envelope approximation (SVEA) in the expression of the Hamiltonian. Furthermore, the model incorporates all the relaxation terms in the equations of motion.

Although the two-level model includes all known physical terms, the ability to test the theoretical model with experiments is challenging due to experimentally having to overcome the hurdle of preparing initially the two-level system into a uniform coherent state throughout the sample—as the exciting pulse used to put the system into a nearly inverted state is strongly absorbed as it propagates in the slab (the linear optics absorption length in this medium is equal to a small fraction ($\approx \frac{1}{7}$) of a wavelength in a homogeneously broadened medium.) In order to avoid this experimental difficulty, one may consider instead of the two-level atoms system an ensemble of three-level cascade atoms [5–7], with levels nearly equidistant (an example of such a system is $6S_{1/2}$, $6P_{1/2}$, $6\ D_{3/2}$ in Cs), and prepare it in the desired initial coherent state of the lowest and highest energy levels through ultrafast two-photons excitation. This method of sample preparation was used by the Hartmann group in their study of yoked super-radiance in Cs [8,9].

However, given the generally different dynamics of the super-radiant emission in two- and three-level systems shown in [10], *a priori*, there is no reason to believe that the cooperative phenomena of forward-backward asymmetry observed in the two-level atomic system would also replicate in three-level atomic systems; and should this asymmetry indeed occur, it will manifest itself in the upper and/or lower transitions' super-radiant emissions.

The goal of this paper is to compute, for the cascade three-level system, the initial conditions that will lead to swings in the direction of super-radiant emission. The highly accurate numerical calculations performed show that the direction of emission of the super-radiant pulse originating from the decay from the intermediate to the ground states of the three-level atoms is extremely sensitive to the value of the initial atomic excitation for slabs with thickness equal to $n\lambda_0/2$ (n is an integer and λ_0 is the wavelength of the lower atomic transition) in the regime of nearly complete inversion (i.e., in the proximity of the value of the initial population of the highest energy atomic level $\chi = 1$). I find, for $n = 3$, that the ratio of the forward to backward fluxes can flip from a value of 0.1302 to a value of 5.511 for a change in the value of χ from 0.9976 to 0.999 968.

This paper is organized as follows: In Sec. II, I review the system of coupled Maxwell-Bloch partial differential equations that govern the dynamics of the three-level system; in Sec. III, I summarize the important properties of the basis functions that would permit one to reduce the mathematical system of partial differential equations into an infinite set of ordinary differential equations; in Sec. IV, I relate the expansion coefficients of the electric field to those of the atomic off-diagonal atomic matrix elements; in Sec. V, I summarize the numerical results obtained for the ratio of the forward to backward fluxes in the different ranges of the initial excitation and show that the unique feature for the forward-backward emission asymmetry exists for the lower transition emission for the case that the slab thickness is equal to $n\lambda_0/2$. In the Appendix, I give the explicit expressions of the coupled ordinary differential equations in time that

*jmanassah@gmail.com

govern the dynamical development of the atomic density matrix expansion coefficients.

II. THE MAXWELL-BLOCH SYSTEM

In this section, I review the expressions for the set of Maxwell-Bloch equations for the cascade three-level system.

I define the normalized lengths for a slab of thickness $2\,z_0$ as follows: $Z = z/z_0$, $u_0 = k_0 z_0$, where $k_0 = 2\pi/\lambda_0$, and λ_0 is the wavelength of the atomic transition.

The designation of the different atomic levels is such that $E_c > E_b > E_a$. I assume that the transition between level c and level b is dipolar and that the transition between level b and level a is also dipolar; furthermore, I am assuming that the two transition dipoles are equal to $\wp$. Finally, in the present model, the dipolar transition, between level c and level a, is assumed to be forbidden.

The normalized electric fields corresponding to the two transitions are given, respectively, by $\psi_{cb} = \wp\varepsilon_{cb}/\hbar C$, and $\psi_{ba} = \wp\varepsilon_{ba}/\hbar C$ where ε_{cb} and ε_{ba} are the transition fields and C is the parameter of interatomic cooperativity $C = \frac{4\pi N \wp^2}{\hbar V}$ (N is the number of atoms, V is the slab volume, and $\wp$ is the reduced dipole moment of the atomic transition. The isolated atom decay rate is given by $\gamma_1 = \frac{4}{3}\,\wp^2\,k_0^3\,/\hbar$).

The Bloch equations for the system are [10]

$$\frac{\partial \rho_{aa}}{\partial T} = \Gamma_{ba}\rho_{bb} - i\psi_{ba}\rho^*_{ba} + i\psi^*_{ba}\rho_{ba}, \tag{1}$$

$$\frac{\partial \rho_{bb}}{\partial T} = -\Gamma_{ba}\rho_{bb} + \Gamma_{cb}\rho_{cc} + i\psi_{ba}\rho^*_{ba} - i\psi^*_{ba}\rho_{ba} - i\psi_{cb}\rho^*_{cb} + i\psi^*_{cb}\rho_{cb}, \tag{2}$$

$$\frac{\partial \rho_{cc}}{\partial T} = -\Gamma_{cb}\rho_{cc} + i\psi_{cb}\rho^*_{cb} - i\psi^*_{cb}\rho_{cb}, \tag{3}$$

$$\frac{\partial \rho_{cb}}{\partial T} = -(\gamma_{cb} + i\,\Delta_{cb})\rho_{cb} - i\psi^L_{cb}(\rho_{cc} - \rho_{bb}) - i\psi^{L*}_{ba}\rho_{ca}, \tag{4}$$

$$\frac{\partial \rho_{ba}}{\partial T} = -(\gamma_{ba} + i\,\Delta_{ba})\rho_{ba} - i\psi^L_{ba}(\rho_{bb} - \rho_{aa}) + i\psi^{L*}_{cb}\rho_{ca}, \tag{5}$$

$$\frac{\partial \rho_{ca}}{\partial T} = -(\gamma_{ca} + i\,\Delta_{cb} + i\,\Delta_{ba})\rho_{ca} - i\psi^L_{ba}\rho_{cb} + i\psi^L_{cb}\rho_{ba}, \tag{6}$$

where the superscript L refers to the local field (as opposed to the Maxwell field which is not superscripted), the Γ's are the normalized decay constants, which will be assumed in the numerical calculations to be ($= 0.05\,a$) where a is the constant in the expressions of the γ's, the transverse decay times, due to collisions; and T is the retarded time normalized to the cooperativity parameter.

The transverse decay rates are given by the expressions [11]

$$\gamma_{cb} = a(\rho_{cc} + \rho_{bb}), \tag{7a}$$

$$\gamma_{ba} = a(\rho_{bb} + \rho_{aa}), \tag{7b}$$

$$\gamma_{ca} = 0. \tag{7c}$$

The Maxwell and local fields are related through [11]

$$\psi^L_{cb} = \psi_{cb} + \tfrac{1}{3}\rho_{cb}, \tag{8a}$$

$$\psi^L_{ba} = \psi_{ba} + \tfrac{1}{3}\rho_{ba}. \tag{8b}$$

For small samples (i.e., the transit time of light across the sample thickness is much smaller than the typical system relaxation times) Maxwell equations for the normalized transition fields are given, respectively, by

$$\psi_{cb}(Z,T) = iu_0\int_{-1}^{1} dZ'\rho_{cb}(Z,T)\exp(iu_0|Z-Z'|), \tag{9}$$

$$\psi_{ba}(Z,T) = iu_0\int_{-1}^{1} dZ'\rho_{ba}(Z,T)\exp(iu_0|Z-Z'|). \tag{10}$$

III. BASIS FUNCTIONS

The basis functions are chosen to be the eigenfunctions of the integral equation:

$$\Lambda_s\varphi_s(Z) = \frac{u_0}{2}\int_{-1}^{1} dZ'\exp(iu_0|Z-Z'|)\varphi_s(Z'), \tag{11}$$

where the kernel of this integral equation is the Liénard-Wiechert Green's function in one-space dimension.

This integral equation's eigenfunctions belong to one of two families (odd, even).

The expressions of the normalized eigenfunctions are, respectively,

$$\tilde{\varphi}^o_m(Z) = \frac{1}{\sqrt{N^o_m}}\sin\left(v^o_m Z\right), \tag{12a}$$

$$\tilde{\varphi}^e_m(Z) = \frac{1}{\sqrt{N^e_m}}\cos\left(v^e_m Z\right), \tag{12b}$$

where the normalization constants are

$$N^o_s = 1 - \frac{\cos^2\left(v^o_s\right)}{iu_0}, \tag{13a}$$

$$N^e_s = 1 - \frac{\sin^2\left(v^e_s\right)}{iu_0}, \tag{13b}$$

and the wave vectors (v^0_s, v^e_s) are solutions of the transcendental equations

$$\cot\left(v^0_s\right) = i\,\frac{u_0}{v^o_s}, \tag{14a}$$

$$\tan\left(v^e_s\right) = -i\,\frac{u_0}{v^e_s}. \tag{14b}$$

The integral equation eigenvalues are given by

$$\Lambda^{o,e}_s = \frac{iu_0^2}{u_0^2 - \left(v^{o,e}_s\right)^2}. \tag{15}$$

The integral equation eigenfunctions obey pseudo-orthonormal relations and form a complete set of basis functions for all functions over the interval: $-1 \leqslant Z \leqslant 1$ [5].

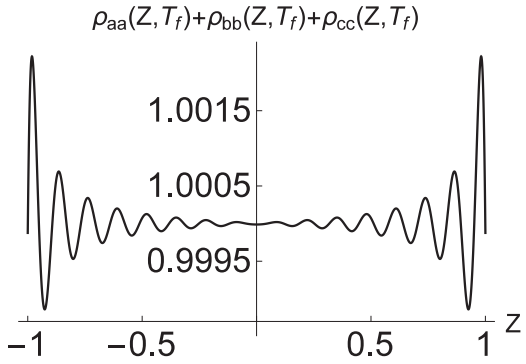

FIG. 1. The trace of the density matrix is plotted as a function of the normalized position in the slab for $T = T_f$; $u_0 = \frac{3\pi}{2}$; $\chi = 0.999\,999\,9$.

Using the reduction technique familiar from the Fourier series methodology, the set of partial differential equations forming the Maxwell-Bloch system for this atomic configuration, as given in Sec. II [10], is then reduced using the above basis to an infinite set of ordinary differential equations (ODEs) in normalized time for the dynamical variables expansion components. This set of derived coupled first-order ODEs is subsequently solved by standard numerical techniques.

In the next section, I shall define the expansion coefficients of the electric field and for the different atomic density matrix elements, and derive the identities that relate the expansion coefficients of the Maxwell fields with those of the atomic off-diagonal matrix elements.

IV. THE EXPANSION COEFFICIENTS OF THE DYNAMICAL VARIABLES

The expansion coefficients of the different dynamical variables are defined through

$$\psi_{cb}(Z,T) = \sum_s e^o_{cb,\,s}(T)\tilde{\varphi}^o_s(Z) + \sum_s e^e_{cb,\,s}(T)\tilde{\varphi}^e_s(Z), \quad (16a)$$

$$\psi_{ba}(Z,T) = \sum_s e^o_{ba,\,s}(T)\tilde{\varphi}^o_s(Z) + \sum_s e^e_{ba,\,s}(T)\tilde{\varphi}^e_s(Z), \quad (16b)$$

$$\rho_{xy}(Z,T) = \sum_s r^o_{xy,\,s}(T)\tilde{\varphi}^o_s(Z) + \sum_s r^e_{xy,\,s}(T)\tilde{\varphi}^e_s(Z), \quad (16c)$$

where the subscript xy stands for aa,bb,cc,ca,cb,ba, and the normalized time $T = Ct_{\rm ret}$.

Combining Eqs. (9) and (10) with Eq. (11), one obtains the following relations between the expansion coefficients of the electric Maxwell fields and those of the off-diagonal atomic density matrix elements:

$$e^{o,e}_{cb,\,s}(T) = i\,2\,\Lambda_s r^{o,e}_{cb,\,s}(T), \quad (17a)$$

$$e^{o,e}_{ba,\,s}(T) = i\,2\,\Lambda_s r^{o,e}_{ba,\,s}(T). \quad (17b)$$

The expansion coefficients for the local fields (the electric fields that should be used in Bloch equations) are related to those of the Maxwell fields through [11,12]

$$\epsilon^{o,e}_{cb,s} = e^{o,e}_{cb,\,s} + \tfrac{1}{3} r^{o,e}_{cb,\,s}, \quad (18a)$$

$$\epsilon^{o,e}_{ba,s} = e^{o,e}_{ba,\,s} + \tfrac{1}{3} r^{o,e}_{ba,\,s}, \quad (18b)$$

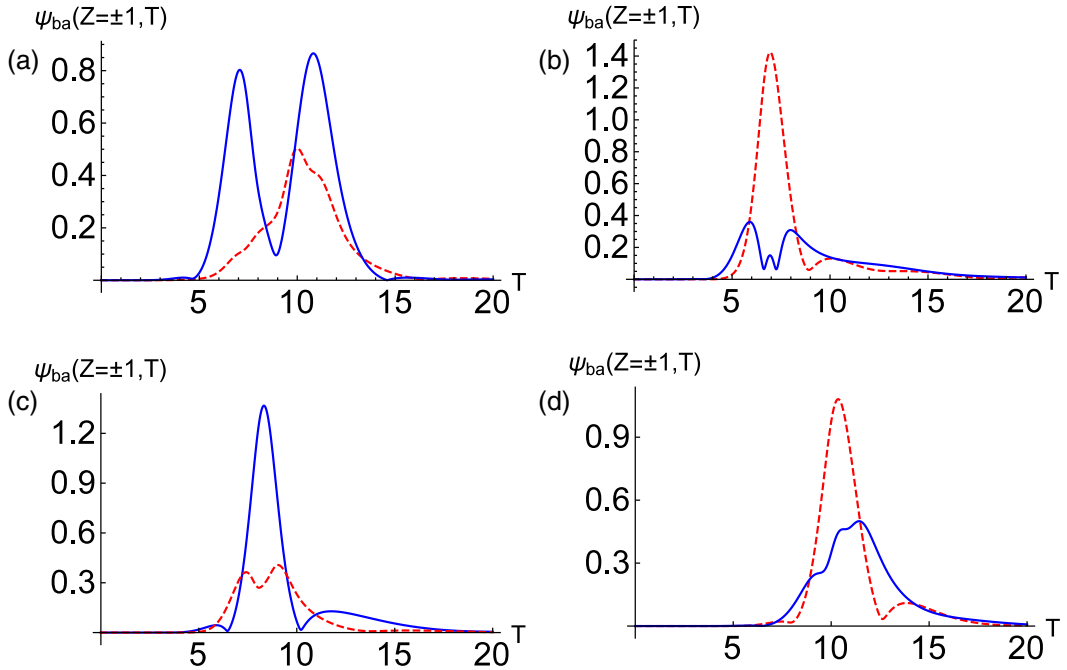

FIG. 2. The magnitude of the normalized lower transition field at the front end (solid line) and the back end (dashed line) of the slab are plotted as a function of the normalized time ($u_0 = \frac{3\pi}{2}$). (a) $\chi = 0.9$; (b) $\chi = 0.9976$; (c) $\chi = 0.999\,968$; (d) $\chi = 0.999\,999\,9$.

where the ϵ's refer to the expansion coefficients of the local fields.

Using Eqs. (18a) and (18b), Bloch equations can be written entirely as an infinite set of coupled ordinary differential equations in the expansion coefficients of the different atomic density matrix elements (i.e., the explicit dependence on the electric fields expansion coefficients has been eliminated). These sets of coupled differential equations are given in the Appendix.

The following initial conditions are used for the expansion coefficients at initial time ($T = 0$), for the case considered of two-photon coherent excitation:

$$r^e_{cc,s}(T=0) = \chi \int_{-1}^{1} dZ \tilde{\varphi}^e_s(Z) = \frac{2\chi}{\sqrt{N^e_s}} \frac{\sin\left(v^e_s\right)}{v^e_s}, \tag{19a}$$

$$r^e_{aa,s}(T=0) = (1-\chi) \int_{-1}^{1} dZ \tilde{\varphi}^e_s(Z) = \frac{2(1-\chi)}{\sqrt{N^e_s}} \frac{\sin\left(v^e_s\right)}{v^e_s}, \tag{19b}$$

$$r^o_{ca,s}(T=0) = \sqrt{\chi(1-\chi)} \int_{-1}^{1} dZ \frac{\sin\left(v^o_s Z\right)}{\sqrt{N^o_s}} \exp\left(i\kappa Z\right)$$

$$= \frac{\sqrt{\chi(1-\chi)}}{i\sqrt{N^o_s}} \left[\frac{\sin\left(\kappa + v^o_s\right)}{\left(\kappa + v^e_s\right)} - \frac{\sin\left(\kappa - v^o_s\right)}{\left(\kappa - v^o_s\right)} \right], \tag{19c}$$

$$r^e_{ca,s}(T=0) = \sqrt{\chi(1-\chi)} \int_{-1}^{1} dZ \frac{\cos\left(v^e_s Z\right)}{\sqrt{N^e_s}} \exp\left(i\kappa Z\right)$$

$$= \frac{\sqrt{\chi(1-\chi)}}{\sqrt{N^e_s}} \left[\frac{\sin\left(\kappa + v^e_s\right)}{\left(\kappa + v^e_s\right)} + \frac{\sin\left(\kappa - v^e_s\right)}{\left(\kappa - v^e_s\right)} \right], \tag{19d}$$

where $\kappa = 2$. (These quantities correspond to the initial conditions

$$\rho_{cc}(Z, T=0) = \chi, \quad \rho_{bb}(Z, T=0) = 0,$$

$$\rho_{aa}(Z, T=0) = (1-\chi),$$

$$\rho_{ca}(Z, T=0) = \sqrt{\chi(1-\chi)} \exp\left(i\kappa Z\right).$$

The values of all other density matrix elements expansion coefficients at $T = 0$ are set equal to zero.

V. NUMERICAL RESULTS

The normalized electric fields (Rabi frequencies) as a function of the normalized time at the front-end and the backward-end planes for an arbitrary initial value of the population difference are given by

$$\psi_{cb}(Z = \pm 1, T) = 2i \left[\sum_s \Lambda^e_s r^e_{cb,\,s}(T) \frac{\cos\left(v^e_s\right)}{\sqrt{N^e_s}} \pm \sum_s \Lambda^o_s r^o_{cb,\,s}(T) \frac{\sin\left(v^o_s\right)}{\sqrt{N^o_s}} \right], \tag{20a}$$

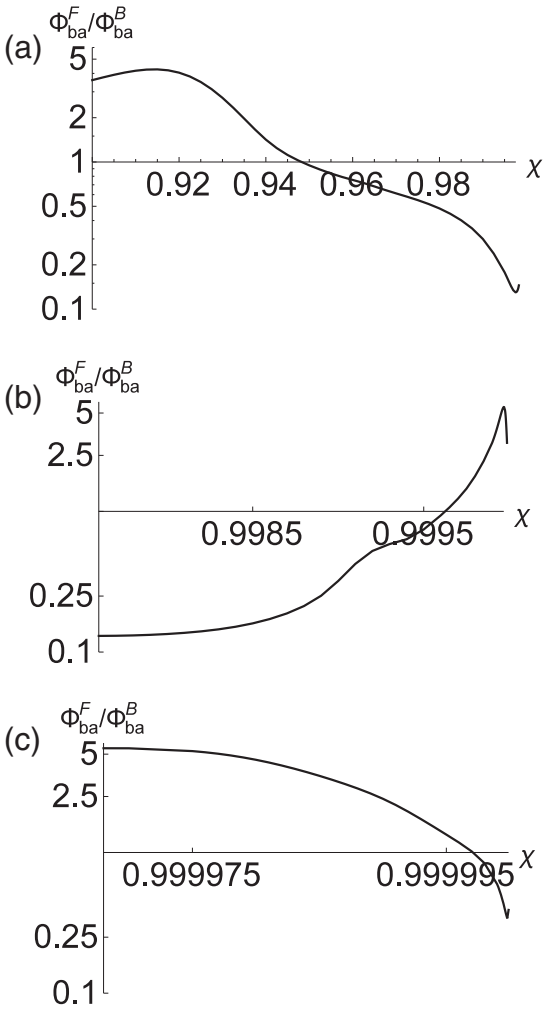

FIG. 3. For $u_0 = \frac{3\pi}{2}$, the ratio of the lower transition forward flux over the backward flux is plotted as a function of χ, the initial population of the upper state for the intervals (a) $0.9 \leqslant \chi \leqslant 0.9976$; (b) $0.9976 \leqslant \chi \leqslant 0.999\,968$; (c) $0.999\,968 \leqslant \chi \leqslant 0.999\,999\,9$.

$$\psi_{ba}(Z = \pm 1, T) = 2i \left[\sum_s \Lambda^e_s r^e_{ba,\,s}(T) \frac{\cos\left(v^e_s\right)}{\sqrt{N^e_s}} \pm \sum_s \Lambda^o_s r^o_{ba,\,s}(T) \frac{\sin\left(v^o_s\right)}{\sqrt{N^o_s}} \right]. \tag{20b}$$

In the subsequent numerical computations, I approximate the infinite dimensional basis functions by the finite functions space spanned by the first 16 even and 16 odd eigenfunctions, and I took the normalized-time window to be the interval $T \in [0,\, T_f = 200]$.

In order to illustrate the accuracy of the above algorithm, using the above finite dimensional basis and the selected time window, I computed the sum of the three density matrix diagonal elements as a function of the normalized distance at $T = T_f$.

In Fig. 1, I show the numerical results of these computations for the following value: $\chi = 0.999\,999\,9$. (This is the case with the largest deviation of the numerical results from the exact value 1; giving an upper limit on the errors equal to less than two parts per thousand.)

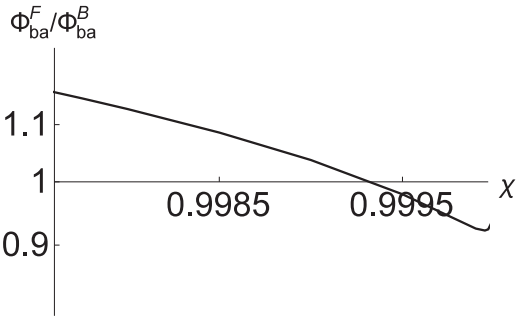

FIG. 4. For $u_0 = \frac{7\pi}{4}$, the ratio of the lower transtion forward flux over the backward flux is plotted as a function of χ, the initial population of the upper state for the interval $0.9976 \leqslant \chi \leqslant 0.999\,968$.

In Fig. 2, I plot the normalized electric field for the lower transition at the end planes of the slab, for $u_0 = \frac{3\pi}{2}$, for the respective values $\chi = 0.9$, $\chi = 0.9976$, $\chi = 0.999\,968$, and $\chi = 0.999\,999\,9$. One notes the swings in the dominant emission direction of the super-radiant pulse. Furthermore, one notes the decrease in the variation required in the value of the initial population in order to affect a flip in the emission direction to occur for $\chi \to 1$.

In Fig. 3, I plot the ratio of the forward to backward time integrated normalized field intensities (the fluxes) for the lower transition emission in the intervals separating the values of the initial population of Fig. 2. Note, for instance, that this ratio goes from the value 0.130 for $\chi = 0.9976$ to the value 5.51 for $\chi = 0.999\,968$.

To illustrate the exceptionality of the flip-flop observed in the ratio of the forward to backward fluxes of the lower transition emission, for $u_0 = \frac{n\pi}{2}$, I plot in Fig. 4 this same ratio for the same interval as that shown in Fig. 3(b) but now for $u_0 = \frac{7\pi}{4}$. One notes that the change in the value of the ratio of the fluxes varies in this later case by less than 25% throughout the whole interval.

In Fig. 5, I plot the ratio of the fluxes for the upper transition emission for the same ranges as in Fig. 3. One notices that the large swings observed in Fig. 3 are absent in this case, from which one makes the observation that qualitatively the lower transition emission in the cascade three-level system is the one that bears more resemblance to the super-radiance emission in the two-level model.

In the above calculations, I showed that for the lower transition super-radiant signal, the ratio of the forward flux over the backward flux changes drastically, in an initially nearly inverted ensemble of three-level cascade atoms prepared in a coherent state of the lowest and highest levels, for small changes in the initial population of the highest level. These substantial changes in the ratio of the forward to backward flux by nearly two orders of magnitudes occur if the slab thickness is a multiple of the half-wavelength of the atomic transition. The physical effect observed here is akin to constructive and destructive interferences in the fields amplitude having their root in the existence of two eigenvalues of the Liénard-Wiechert 1D kernel having equal real parts in the case that

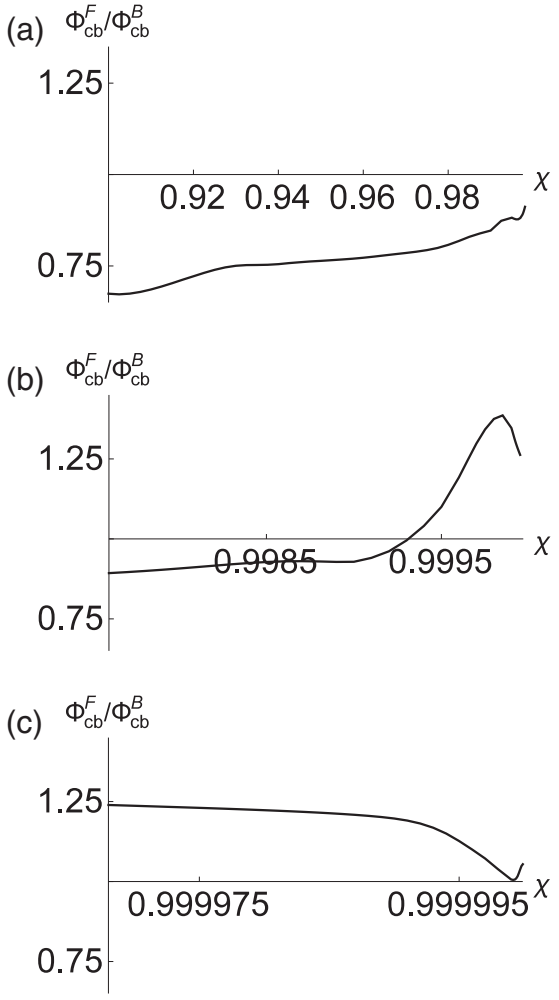

FIG. 5. For $u_0 = \frac{3\pi}{2}$, the ratio of the upper transition forward flux over the backward flux is plotted as a function of χ, the initial population of the upper state for the interval (a) $0.9 \leqslant \chi \leqslant 0.9976$; (b) $0.9976 \leqslant \chi \leqslant 0.999\,968$; (c) $0.999\,968 \leqslant \chi \leqslant 0.999\,999\,9$.

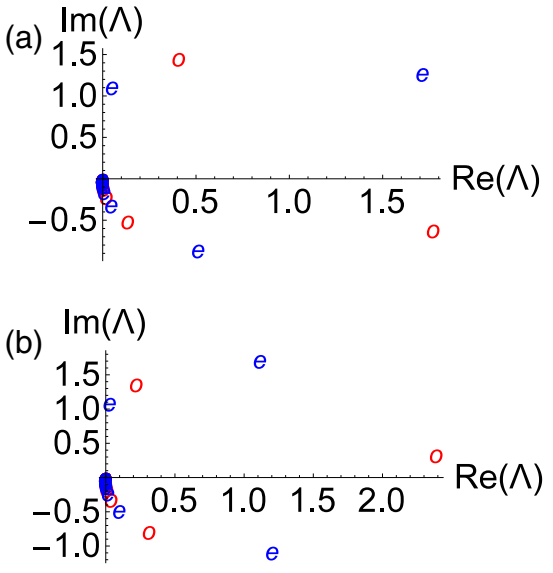

FIG. 6. The loci in the complex plane of the eigenvalues of the 1D Liénard-Wiechert kernel. ("o" refers to the odd family of eigenfunctions, "e" refers to the even families of eigenfunctions) (a) $u_0 = \frac{3\pi}{2}$; (b) $u_0 = \frac{7\pi}{4}$.

the thickness of the sample is a multiple of half the transition wavelength. I show in Fig. 6 the loci of the eigenvalues for the two values of the thickness considered in Figs. 3 and 4, and note that only in Fig. 6(a) there is degeneracy in the real part of the dominant eigenvalues.

The existence of the forward-backward asymmetry in only the lower transition reflects the general property, studied in detail in [10], where we showed that the behavior of only the lower transition in the cascade system is akin to those observed in the two-level system.

APPENDIX

Using the pseudo-orthogonal property of the eigenfunctions of the non-Hermitian kernel of the 1D Liénard-Wiechert kernel [3], Eqs. (17a) and (17b) and Bloch equations [Eqs. (1)–(6)], it is straightforward to derive the set of coupled ordinary different equations describing the dynamics of the different expansion coefficients, namely,

$$\frac{dr^{o}_{aa,n}}{dT} = \Gamma_{ba} r^{o}_{bb,n} - i \sum_{p,q} \left\{ \left[E_2(n,p,q) \epsilon^{o}_{ba,p} r^{e^*}_{ba,q} + F_2(n,p,q) \epsilon^{e}_{ba,p} r^{o^*}_{ba,q} \right] - \left[E_1(n,p,q) \epsilon^{o^*}_{ba,p} r^{e}_{ba,q} + F_1(n,p,q) \epsilon^{e^*}_{ba,p} r^{o}_{ba,q} \right] \right\}, \tag{A1}$$

$$\frac{dr^{e}_{aa,n}}{dT} = \Gamma_{ba} r^{e}_{bb,n} - i \sum_{p,q} \left\{ \left[H_1(n,p,q) \epsilon^{o}_{ba,p} r^{o^*}_{ba,q} + H_2(n,p,q) \epsilon^{e}_{ba,p} r^{e^*}_{ba,q} \right] - \left[G_1(n,p,q) \epsilon^{o^*}_{ba,p} r^{o}_{ba,q} + G_2(n,p,q) \epsilon^{e^*}_{ba,p} r^{e}_{ba,q} \right] \right\}, \tag{A2}$$

$$\begin{aligned} \frac{dr^{o}_{bb,n}}{dT} = & - \Gamma_{ba} r^{o}_{bb,n} + \Gamma_{cb} r^{o}_{cc,n} + i \sum_{p,q} \left\{ \left[E_2(n,p,q) \epsilon^{o}_{ba,p} r^{e^*}_{ba,q} + F_2(n,p,q) \epsilon^{e}_{ba,p} r^{o^*}_{ba,q} \right] \right. \\ & - \left[E_1(n,p,q) \epsilon^{o^*}_{ba,p} r^{e}_{ba,q} + F_1(n,p,q) \epsilon^{e^*}_{ba,p} r^{o}_{ba,q} \right] - \left[E_2(n,p,q) \epsilon^{o}_{cb,p} r^{e^*}_{cb,q} + F_2(n,p,q) \epsilon^{e}_{cb,p} r^{o^*}_{cb,q} \right] \\ & \left. + \left[E_1(n,p,q) \epsilon^{o^*}_{cb,p} r^{e}_{cb,q} + F_1(n,p,q) \epsilon^{e^*}_{cb,p} r^{o}_{cb,q} \right] \right\}, \end{aligned} \tag{A3}$$

$$\begin{aligned} \frac{dr^{e}_{bb,n}}{dT} = & - \Gamma_{ba} r^{e}_{bb,n} + \Gamma_{cb} r^{e}_{cc,n} + i \sum_{p,q} \left\{ \left[H_1(n,p,q) \epsilon^{o}_{ba,p} r^{o^*}_{ba,q} + H_2(n,p,q) \epsilon^{e}_{ba,p} r^{e^*}_{ba,q} \right] \right. \\ & - \left[G_1(n,p,q) \epsilon^{o^*}_{ba,p} r^{o}_{ba,q} + G_2(n,p,q) \epsilon^{e^*}_{ba,p} r^{e}_{ba,q} \right] - \left[H_1(n,p,q) \epsilon^{o}_{cb,p} r^{o^*}_{cb,q} + H_2(n,p,q) \epsilon^{e}_{cb,p} r^{e^*}_{cb,q} \right] \\ & \left. + \left[G_1(n,p,q) \epsilon^{o^*}_{cb,p} r^{o}_{cb,q} + G_2(n,p,q) \epsilon^{e^*}_{cb,p} r^{e}_{cb,q} \right] \right\}, \end{aligned} \tag{A4}$$

$$\frac{dr^{o}_{cc,n}}{dT} = -\Gamma_{cb} r^{o}_{cc,n} + i \sum_{p,q} \left\{ \left[E_2(n,p,q) \epsilon^{o}_{cb,p} r^{e^*}_{cb,q} + F_2(n,p,q) \epsilon^{e}_{cb,p} r^{o^*}_{cb,q} \right] - \left[E_1(n,p,q) \epsilon^{o^*}_{cb,p} r^{e}_{cb,q} + F_1(n,p,q) \epsilon^{e^*}_{cb,p} r^{o}_{cb,q} \right] \right\}, \tag{A5}$$

$$\frac{dr^{e}_{cc,n}}{dT} = -\Gamma_{cb} r^{e}_{cc,n} + i \sum_{p,q} \left\{ \left[H_1(n,p,q) \epsilon^{o}_{cb,p} r^{o^*}_{cb,q} + H_2(n,p,q) \epsilon^{e}_{cb,p} r^{e^*}_{cb,q} \right] - \left[G_1(n,p,q) \epsilon^{o^*}_{cb,p} r^{o}_{cb,q} + G_2(n,p,q) \epsilon^{e^*}_{cb,p} r^{e}_{cb,q} \right] \right\}, \tag{A6}$$

$$\begin{aligned} \frac{dr^{o}_{cb,n}}{dT} = & -i \Delta_{cb} r^{o}_{cb,n} - a \sum_{p,q} \left[A(n,p,q) \left(r^{o}_{bb,p} + r^{o}_{cc,p} \right) r^{e}_{cb,q} + B(n,p,q) \left(r^{e}_{bb,p} + r^{e}_{cc,p} \right) r^{o}_{cb,q} \right] \\ & - i \sum_{p,q} \left\{ \left[A(n,p,q) \epsilon^{o}_{cb,p} \left(r^{e}_{cc,q} - r^{e}_{bb,q} \right) + B(n,p,q) \epsilon^{e}_{cb,p} \left(r^{o}_{cc,q} - r^{o}_{bb,q} \right) \right] \right. \\ & \left. + \left[E_1(n,p,q) \epsilon^{o^*}_{ba,p} r^{e}_{ca,q} + F_1(n,p,q) \epsilon^{e^*}_{ba,p} r^{o}_{ca,q} \right] \right\}, \end{aligned} \tag{A7}$$

$$\begin{aligned} \frac{dr^{e}_{cb,n}}{dT} = & -i \Delta_{cb} r^{e}_{cb,n} - a \sum_{p,q} \left[C(n,p,q) \left(r^{o}_{bb,p} + r^{o}_{cc,p} \right) r^{o}_{cb,q} + D(n,p,q) \left(r^{e}_{bb,p} + r^{e}_{cc,p} \right) r^{e}_{cb,q} \right] \\ & - i \sum_{p,q} \left\{ \left[C(n,p,q) \epsilon^{o}_{cb,p} \left(r^{o}_{cc,q} - r^{o}_{bb,q} \right) + D(n,p,q) \epsilon^{e}_{cb,p} \left(r^{e}_{cc,q} - r^{e}_{bb,q} \right) \right] \right. \\ & \left. + \left[G_1(n,p,q) \epsilon^{o^*}_{ba,p} r^{o}_{ca,q} + G_2(n,p,q) \epsilon^{e^*}_{ba,p} r^{e}_{ca,q} \right] \right\}, \end{aligned} \tag{A8}$$

$$\frac{dr^{o}_{ba,n}}{dT} = -i\ \Delta_{ba} r^{o}_{ba,n} - a \sum_{p,q} \left[A(n,p,q)\left(r^{o}_{bb,p} + r^{o}_{cc,p}\right) r^{e}_{ba,q} + B(n,p,q)\left(r^{e}_{bb,p} + r^{e}_{cc,p}\right) r^{o}_{ba,q} \right]$$

$$- i \sum_{p,q} \left\{ \left[A(n,p,q)\epsilon^{o}_{ba,p}\left(r^{e}_{bb,q} - r^{e}_{aa,q}\right) + B(n,p,q)\epsilon^{e}_{ba,p}\left(r^{o}_{bb,q} - r^{o}_{aa,q}\right) \right] \right.$$

$$\left. - \left[E_1(n,p,q)\epsilon^{o^*}_{cb,p} r^{e}_{cb,q} + F_1(n,p,q)\epsilon^{e^*}_{cb,p} r^{o}_{cb,q} \right] \right\}, \tag{A9}$$

$$\frac{dr^{e}_{ba,n}}{dT} = -i\ \Delta_{ba} r^{e}_{ba,n} - a \sum_{p,q} \left[C(n,p,q)\left(r^{o}_{bb,p} + r^{o}_{cc,p}\right) r^{o}_{ba,q} + D(n,p,q)\left(r^{e}_{bb,p} + r^{e}_{cc,p}\right) r^{e}_{ba,q} \right]$$

$$- i \sum_{p,q} \left\{ \left[C(n,p,q)\epsilon^{o}_{ba,p}\left(r^{o}_{bb,q} - r^{o}_{aa,q}\right) + D(n,p,q)\epsilon^{e}_{ba,p}\left(r^{e}_{bb,q} - r^{e}_{aa,q}\right) \right] \right.$$

$$\left. + \left[G_1(n,p,q)\epsilon^{o^*}_{cb,p} r^{o}_{cb,q} + G_2(n,p,q)\epsilon^{e^*}_{cb,p} r^{e}_{cb,q} \right] \right\}, \tag{A10}$$

$$\frac{dr^{o}_{ca,n}}{dT} = -i\ (\Delta_{cb} + \Delta_{ba}) r^{o}_{ca,n} - i \sum_{p,q} \left[A(n,p,q)\left(\epsilon^{o}_{ba,p} r^{e}_{cb,q} - \epsilon^{o}_{cb,p} r^{e}_{ba,q}\right) + B(n,p,q)\left(\epsilon^{e}_{ba,p} r^{o}_{cb,q} - \epsilon^{e}_{cb,p} r^{o}_{ba,q}\right) \right], \tag{A11}$$

$$\frac{dr^{e}_{ca,n}}{dT} = -i\ (\Delta_{cb} + \Delta_{ba}) r^{e}_{ca,n} - i \sum_{p,q} \left[C(n,p,q)\left(\epsilon^{o}_{ba,p} r^{o}_{cb,q} - \epsilon^{o}_{cb,p} r^{o}_{ba,q}\right) + D(n,p,q)\left(\epsilon^{e}_{ba,p} r^{e}_{cb,q} - \epsilon^{e}_{cb,p} r^{e}_{ba,q}\right) \right], \tag{A12}$$

where Δ_{cb} and Δ_{ba} are the normalized detuning of the transition fields from the atomic transition frequencies; a is the resonance collision broadening width (assumed in the numerical calculations equal to 0.5764 [11,12]). The coupling constants are overlap integrals of various basis functions given by [13]

$$A(s,m,n) = \int_{-1}^{1} dZ \tilde{\varphi}^{o}_{s}(Z)\tilde{\varphi}^{o}_{m}(Z)\tilde{\varphi}^{e}_{n}(Z), \tag{A13}$$

$$D(s,m,n) = \int_{-1}^{1} dZ \tilde{\varphi}^{e}_{s}(Z)\tilde{\varphi}^{e}_{m}(Z)\tilde{\varphi}^{e}_{n}(Z), \tag{A14}$$

$$E_1(s,m,n) = \int_{-1}^{1} dZ \tilde{\varphi}^{o}_{s}(Z)\tilde{\varphi}^{o^*}_{m}(Z)\tilde{\varphi}^{e}_{n}(Z), \tag{A15}$$

$$E_2(s,m,n) = \int_{-1}^{1} dZ \tilde{\varphi}^{o}_{s}(Z)\tilde{\varphi}^{o}_{m}(Z)\tilde{\varphi}^{e^*}_{n}(Z), \tag{A16}$$

$$G_2(s,m,n) = \int_{-1}^{1} dZ \tilde{\varphi}^{e}_{s}(Z)\tilde{\varphi}^{e^*}_{m}(Z)\tilde{\varphi}^{e}_{n}(Z), \tag{A17}$$

and

$$B(s,\ m,\ n) = A(s,n,m), \tag{A18}$$

$$C(s,\ m,\ n) = A(n,\ m,\ s), \tag{A19}$$

$$F_1(m,\ n,\ s) = E_2(s,\ n,\ m), \tag{A20}$$

$$F_2(s,\ m,\ n) = E_1(s,\ n,\ m), \tag{A21}$$

$$G_1(s,\ m,\ n) = E_1(n,\ m,\ s), \tag{A22}$$

$$H_1(s,\ m,\ n) = E_1(m,\ n,\ s), \tag{A23}$$

$$H_2(s,\ m,\ n) = G_2(s,\ n,\ m). \tag{A24}$$

It is worth pointing out that the method that I am using requires numerical calculations only for finding, for the given geometry, the values of the characteristic wave vectors, and at the last step—the integration of the ODEs. All parameters appearing in the ODEs are obtained in closed form.

[1] R. H. Dicke, Coherence in spontaneous radiation processes, Phys. Rev. **93**, 99 (1954).

[2] R. Friedberg and J. T. Manassah, Eigenfunctions and eigenvalues in superradiance with x-y translational symmetry, Phys. Lett. A **372**, 2787 (2008).

[3] J. T. Manassah, Quantum electrodynamics of two-level atoms in 1D configuration, Adv. At., Mol., Opt. Phys. **63**, 359 (2014).

[4] J. T. Manassah, Numerical demonstration of high sensitivity to initial conditions in solutions of the complete Maxwell-Bloch equations for certain parameters, Phys. Lett. A **379**, 1091 (2015).

[5] J. Okada, K. Ikeda, and M. Matsuoka, Cooperative cascade emission, Opt. Commun. **26**, 189 (1978).

[6] K. Ikeda, J. Okada, and M. Matsuoka, Theory of cooperative cascade emission. 1. Linear stochastic theory, J. Phys. Soc. Jpn. **48**, 1636 (1980).

[7] K. Ikeda, J. Okada, and K. Matsuoka, Theory of cooperative cascade emission. 2. Non-linear evolution, J. Phys. Soc. Jpn. **48**, 1646 (1980).

[8] J. H. Brownell, X. Lu, and S. R. Hartmann, Coherence inhibition in cascade superfluorescence, Laser Phys. **5**, 522 (1995).

[9] J. H. Brownell, X. Lu, and S. R. Hartmann, Yoked Superfluoresence, Phys. Rev. Lett. **75**, 3265 (1995).

[10] J. T. Manassah and I. Gladkova, Superradiant amplification in an optically dense three-level cascade system, Opt. Commun. **179**, 51 (2000).

[11] R. Friedberg, S. R. Hartmann, and J. T. Manassah, Frequency shifts in emission and absorption by resonant systems of two-level atoms, Phys. Rep. C **7**, 101 (1973).

[12] J. T. Manassah, Statistical quantum electrodynamics of resonant atoms, Phys. Rep. **101**, 359 (1983).

[13] J. T. Manassah, Eigenmode analysis of superradiance, Phys. Rev. A **89**, 053815 (2014).